Associated conference: 5th International Small Sample Test Techniques Conference

Conference location: Swansea University, Bay Campus

Conference date: 10th - 12 July 2018

How to cite: Hilal, H., Lancaster, R.J., Jeffs, S.P., & Ednie, L., Boswell, J., Stapleton, D., Baxter, G. 2018. High temperature mechanical deformation of an additive manufactured nickel based superalloy using small scale test methods. *Ubiquity Proceedings*, 1(S1): 21 DOI: https://doi.org/10.5334/uproc.21

Published on: 10 September 2018

High temperature mechanical deformation of an additive manufactured nickel based superalloy using small scale test methods

H. Hilal [1], R.J. Lancaster [1], S.P. Jeffs [1], L. Ednie [1], J. Boswell [2], D. Stapleton [2], G. Baxter [2]

1 Institute of Structural Materials, Bay Campus, Swansea University, Swansea, UK, SA1 8EN
2 Rolls-Royce plc., P.O. Box 31, Derby, UK, DE24 8BJ

[1] 710170@Swansea.ac.uk, S.P.Jeffs@Swansea.ac.uk, R.J.Lancaster@Swansea.ac.uk, 826065@Swansea.ac.uk
[2] John.Boswell@Rolls-Royce.com, David.Stapleton2@Rolls-Royce.com,
[2] Grant.Gibson@Rolls-Royce.com, Gavin.Baxter@Rolls-Royce.com.

Abstract: Nickel based superalloys have been utilised within numerous industrial sectors from power generation to chemical processing plants for over four decades as a result of their ability to retain mechanical properties at arduous temperatures alongside excellent oxidation and corrosion resistance. Within the aerospace industry, they have been primarily used within regions of the gas turbine engine where metal temperatures can often exceed 1000ºC and high temperature deformation mechanics are prominent. Although typically manufactured using traditional wrought and casting methodologies, the aerospace industry has become increasingly interested in the use of Additive Layer Manufacturing (ALM) as a means of fabrication to take advantage of the numerous benefits that ALM has to offer. Detailed characterisation of the structural integrity of components processed via additive processes is a key requirement of the understanding. In this paper, the small punch creep (SPC) test has been applied to samples of a high gamma prime containing nickel-based superalloy manufactured using the laser powder bed fusion (LPBF) process. Several different builds are investigated and ranked, with ALM builds provided in different epitaxial orientations and with contrasting process parameters to help determine the optimal process parameters.

Keywords: nickel superalloy; additive layer manufacturing; small punch testing; creep; process parameters.

1. Introduction

Nickel based superalloys display an impressive range of mechanical properties from high temperature strength and toughness to excellent oxidation/corrosion resistance. It is these physical and mechanical properties that have led to its incorporation within numerous industrial sectors, in particular the aerospace industry where nickel is utilised in up to 40% of the gas turbine engine, primarily in the latter region [1].

Nickel based superalloys comprise of two major phases, namely gamma (γ) and gamma prime (γ') with additional secondary phases such as carbides and borides typically present. Although γ, a continuous matrix of face centered cubic (FCC) structured nickel, is the primary constituent in which additional phases reside, γ' typically acts as the key strengthening phase. This occurs as a result of several mechanisms, the main of which being its ordered $L1_2$ crystal structure of alternating Ni and Al. Given their similarity in terms of stoichiometry, there is a significant degree of directional covalent bonding, giving rise to a strong degree of 'chemical order' [2]. In addition to this strengthening mechanism, γ' precipitates can lead to a mechanism known as precipitation hardening, where hard intermetallic particles present within the disordered FCC matrix impede dislocation movement [3].

Despite the association of γ' with strengthening and therefore, increased high temperature capabilities, there is a trade off in regards to fabricability and weldability. This occurs due to a phenomenon known as ductility dip cracking (DCC), where a drop in ductility is observed at intermediate temperatures. Given this, the development of manufacturing methodologies both pre and post fabrication that can alleviate defect forming mechanisms has become precedent. Although nickel superalloys have been traditionally fabricated using wrought and casting methodologies [4], the aerospace industry has become increasingly interested in the use of alternative manufacturing routes such as powder processing, giving the potential scope for more complex alloy design of alloys containing >44% γ' content.

Additive layer manufacture (ALM) is a novel near-net shape manufacturing technique that utilises high energy heat sources in order to fabricate 2D slices of computer aided design (CAD) data, layer by layer until a full 3D component is produced. Although the innovation for this technology occurred in the late 1980s with stereolithography, it was the medical industry that drove its major development throughout the 1990s and 2000s

with the fabrication of numerous functional medical devices [5]. Despite the various forms of additive manufacturing (AM) utilised within the aerospace industry today for both component repair and manufacture, direct layer deposition (DLD) processes such as laser powder bed fusion (LPBF) have become prominent. LPBF is a multi-weld process that incorporates high-energy lasers in order to melt and fuse powders in a desired 3D geometry as illustrated in Figure 1. This leads to numerous advantageous characteristics and capabilities such as the formation of components with highly complex and intricate design geometries [6].

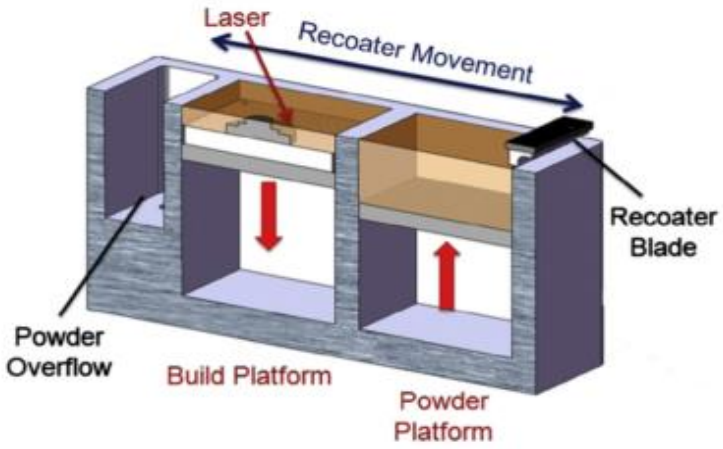

Figure 1. Schematic of LPBF and the Concept Laser M2 recoating system [6].

Regardless of the major advantages of AM in comparison to traditional cast and wrought processing, it has been observed that the frequent presence of material discontinuities needs to be considered, since questions arise regarding structural integrity. As a result of this, there has become an ever increasing importance in gauging a better understanding of how process parameters such as beam speed, power and hatch spacing influence the associated defect forming mechanisms. In addition to these parameters, alternative variables such as build orientation have also been shown to majorly influence mechanical properties as highlighted in numerous papers [7]. It has been hypothesised that a significant enhancement of mechanical properties can be seen when components have build orientations perpendicular to the loading axis. Previous work found that the individual influence of these parameters can be normalized and plotted onto a process map with diagonal isopleths indicating varying degrees of energy density [8]. It has been established that low energy densities are not substantial enough to melt the bulk of powder, leading to high frequencies of void formation. In contrast, higher energy densities are hypothesised to give rise to crack formation mechanisms such as ductility dip cracking (DDC), where a drop in ductility is noticed at intermediate temperatures [9].

In order to characterise builds which will exhibit evolving microstructures throughout, localised mechanical testing methodologies such as small punch testing (SPT) will prove useful. Originally developed within the nuclear industry in the early 1980s, SPT was utilised in order to obtain mechanical property data from small volumes of materials [10]. Given the cost saving implications associated with this alongside localised testing, numerous industrial sectors began to implement this methodology into their arsenal, leading to the resurgence of SPT during the late 1990s and early 2000s when it was successfully utilised to generate creep data [11]. Given the small volume of material required, the aerospace industry has begun to incorporate the use of SPT for the assessment and characterisation of advanced materials such as additively manufactured components, where traditional methodologies such as uniaxial testing may not be possible given design geometries [7].

In SPT, small cylindrical discs of 8-9.5mm diameter and 0.5mm +-0.005mm thickness are subjected to a load via a 2-2.5mm diameter hemi-spherical punch head or ball, either under constant displacement rate or constant load. The selection of which methodology is dependent on what mechanical data is desired. However, given the nature of nickel superalloy usage within the gas turbine engine, high temperature deformation mechanisms such as creep is prominent. As such, small punch creep (SPC) testing is conducted, where the indenter is imparted upon the specimen at a constant load. SPC testing is performed in a ‘dead-weight’ testing arrangement**.** The specimen is circumferentially clamped and restrained between the upper and lower die, otherwise referred to as ‘bulge’ testing. Within this setup, the upper die contains an aperture allowing the puncher to pass through and impose force upon the specimen. Upon plastic deformation which will be onset during primary creep, the specimen will pass and

emerge through the circular 4mm diameter aperture present within the lower die. Heating is then applied through the use of a standard three zone radiant furnace. However, given the high temperatures present, oxidation and corrosion can become prominent. Therefore, it is evident that these tests need to be performed in an inert environment such as argon.

Utilising SPC testing as a means for mechanical characterisation, this paper will explore the influence of process parameters on the microstructural integrity of γ' rich nickel superalloys. Furthermore, the adverse effect of various material discontinuities on mechanical properties will be compared and evaluated.

2. Materials and Methodology

2.1 High Gamma Prime Nickel Superalloys

The alloys of particular interest in this work are polycrystalline high gamma prime nickel superalloys. Although originally intended for utilisiation within directionally solidified blade and vane castings given its exceptional resistance to grand boundary cracking, properties attributed with their coarse grain size [12]. Given its desired application, these alloys coarse grain structure acts as a means of creep enhancement given that grain boundaries are typically susceptible to high temperature creep deformation. This can be achieved through its chemical composition, with the addition of high concentrations of γ' formers, specifically Al + Ti Given the high addition of Al and Ti, high gamma prime alloys contain 50-60% γ' and as a result are sensitive to defect forming mechanisms in AM processing. Figures 2a and 2b showcase both the frequency and distribution of this phase within high volume fractions of γ'. The variation in γ' sizing known as primary, secondary and tertiary γ' can be seen in Figure 2a whilst the distribution of γ', specifically along grain boundaries can be seen in Figure 2b. The presence of γ' along grain boundaries aids a mechanism known as grain boundary pinning, preventing dislocation movement and giving rise to a strengthening effect at a cost for ductility.

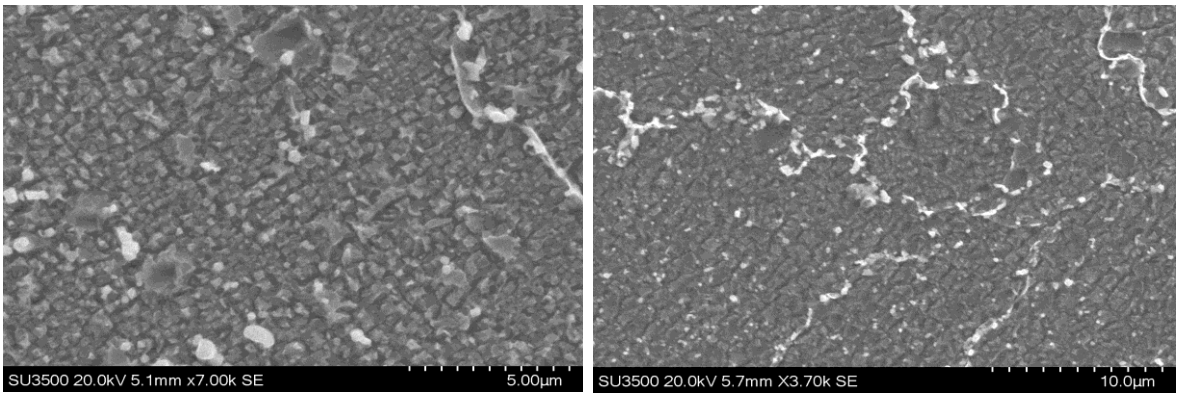

Figure 2. a) CM247LC's high volume fraction of gamma prime (primary, secondary and tertiary), **b)** gamma prime formation and distribution along grain boundaries.

Given the potential scope of high γ' nickel superalloys, there has been on-going work regarding the fabrication of high gamma prime nickel superalloys and as to whether the selection of manufacturing parameters can alleviate the presence of material discontinuities to what is considered a tolerable level. It has been showcased that low energy densities lead to the formation of voids as seen in Figure 3a. It is hypothesised that this occurs as a result of a lack of powder consolidation and therefore lack of complete melting. Conversely, it has been displayed that high energy densities leads to the formation of crack development as seen in Figure 3b**.** As previously mentioned, this has been attributed to DCC, a phenomenon that occurs as a combination of two mechanisms. These include micro stressing as a result of incoherent grain boundary carbides interrupting stoichiometry alongside macro residual stresses induced through welding.

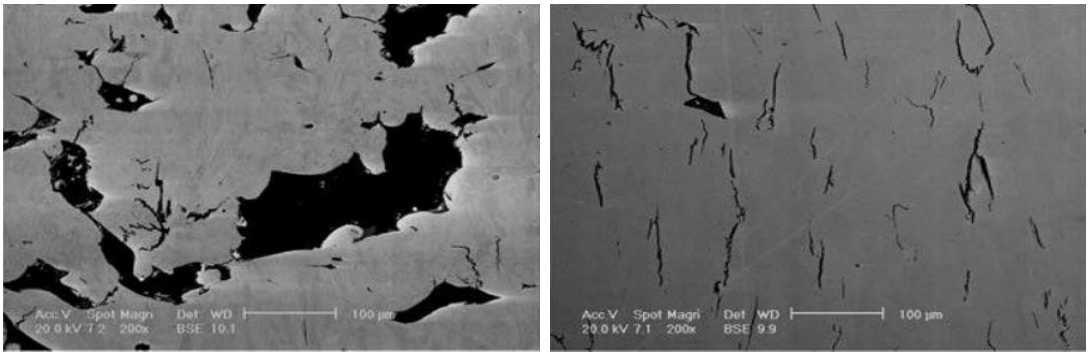

Figure 3. a) Large evidence of voids attributed to a lack of powder consolidation at low energy densities**, b)** high microcracking attributed to DCC witnessed at high energy densities [9].

As previously mentioned, the University of Sheffield developed the Normalised Process Parameters map over a range of alloying systems including nickel, titanium and steel alloys in order to illustrate the influence of combined parameters as depicted in Figure 4. It is worth noting that within this process map, high gamma prime nickel superalloys showxase an extremely limited process window, which is mainly accredited to its poor fabricability as discussed. Energy Density (*E**), as indicated by the diagonal isopleths, is quantified through the following equations:

$$E^* = \frac{q^*}{v^* l^*} = \left[\frac{Aq}{2vlrB}\right]\left[\frac{1}{\rho Cp(Tm-T0)}\right] \qquad \frac{1}{h^*} = \frac{rB}{h}$$

Where q^* = normalized power, v^* = normalized beam velocity, l^* = layer height, a = surface absorptivity, q = power (W), v = beam velocity (ms^{-1}), l = layer height (m), rB = beam radius (m), ρ = density (kgm-3), C_p = specific heat capacity (J Kg K^{-1}), T_m = melting temperature (K), T_0 = initial powder bed temperature (K), h^* = normalised hatch spacing and h = hatch spacing (m).

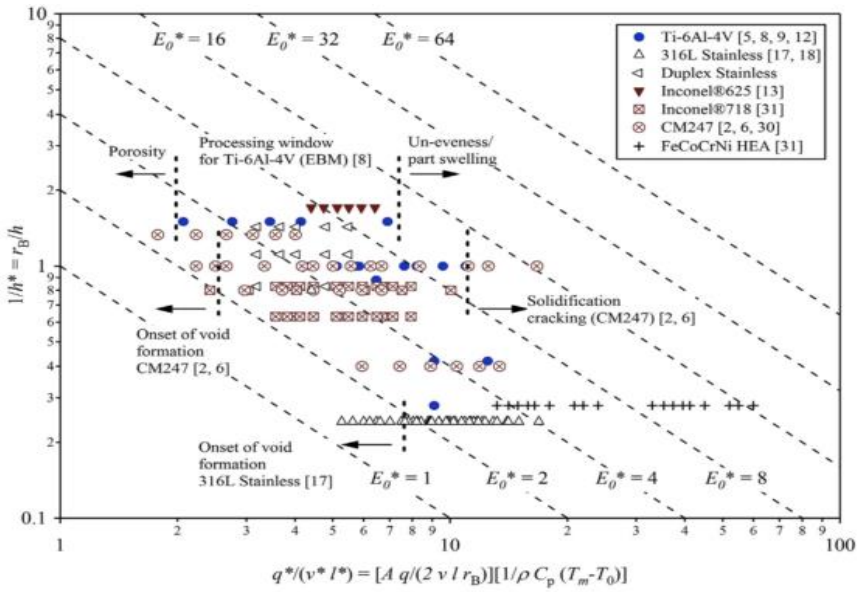

Figure 4. Normalised process parameters map with dimensionless beam power over beam velocity and layer height in comparison to normalized hatch spacing [13].

Given the limited window for processability, samples from the extremities of the window were additively manufactured and mechanically tested in order to gauge an understanding of energy density on mechanical properties. When considering the diagonal isopleths, as can be seen in Figure 4, the top right represents a high energy density with the bottom left being low. The labelling system for the specimens is explained below with the following example:

90-DOE-3-2 Position 1

Where 90 refers to the build orientation (90˚), 3 refers to the parameter set (low energy density), 2 refers to the build number and position 1 refers to post processing conditions (1 HIPed, 2 as built). It is worth noting that for build orientation, samples were extracted from thin plates rather than rods as shown in Figure 5.

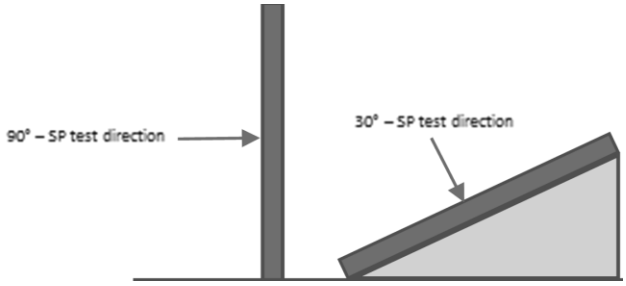

Figure 5. 30 and 90˚ orientation build schematics.

Post manufacturing processing such as heat treatments (HT) and hot isostatic pressing (HIPing) have been shown to have an adverse effect on both microstructure and discontinuities such as porosity and cracking [14]. Heat treatments, in particular can leave cracks and pores in the microstructure. However, when combined with HIPing the microstructure can internally heal cracking as shown below in Figures 6a and 6b. The extended heat treatment has also been shown to develop a coarser grain structure. This paper will compare several additively manufactured builds in as built and HIPed conditions in order to assess whether these processes aid mechanical performance.

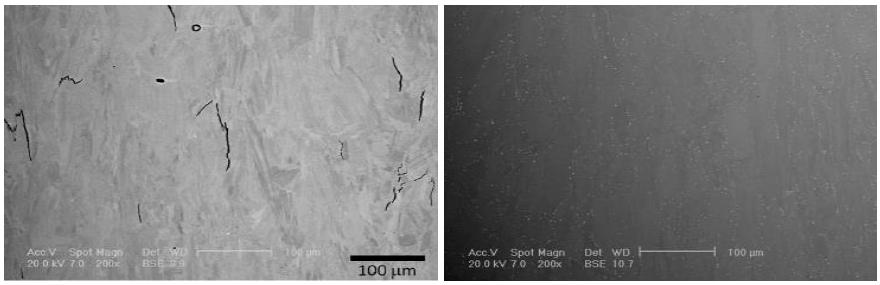

Figure 6. Additive Layer Manufactured nickel superalloys solidification cracks internally 'healed', **a)** before and **b)** after HIPing [14].

2.2 Small Punch Creep Testing

Using a series of grinding papers, samples of 9.5mm diameter, 2.2mm thickness were reduced to 1mm thickness using a 60# paper. From here, the sample was ground down to 0.6mm using a 500# paper, and finally reduced to 0.500mm with tolerances of +- 0.005mm using a 1200# paper. The edges of the sample were also rounded and both sides equally ground down in order to ensure uniformity and prevent beveling. Multiple SPC tests were performed on a modified high temperature SPC frame developed at Swansea University as illustrated in Figure 7a.

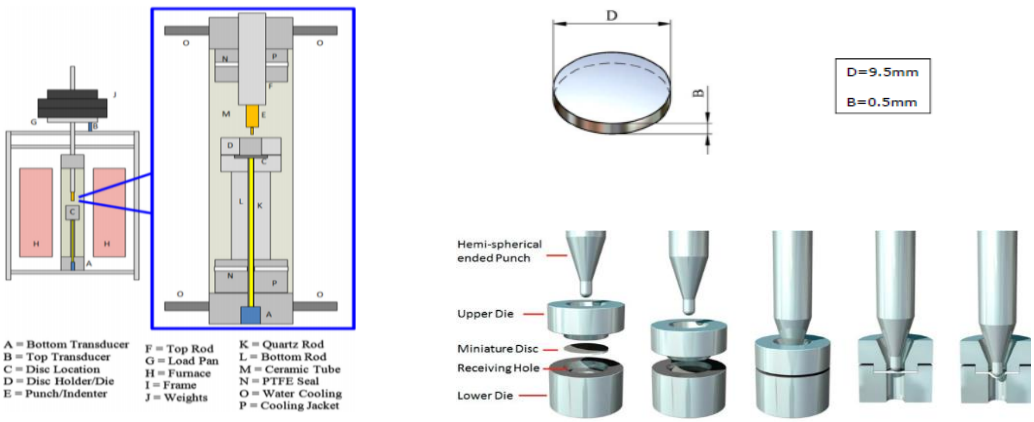

Figure 7. a) SPCT frame developed at Swansea University [15], **b)** SP disc diameters matching the European CoP specifications, **c)** lower and upper die clamping system [16].

The small cylindrical specimens, as shown in Figure 7, match the specifications set forth by the European Code of Practice for Small Punch Testing [17] and were circumferentially clamped within the threaded upper and lower die, with the top rod being aligned centrally to the disc from the above loading pan. Below the top rod, a ceramic indenter with a cylindrical head of 2mm diameter is utilised in order to deform the material under a total constant load of 150N. LVDTs located both underneath the loading pan and the underside of the disc measures and records the displacement/deflection that occurs during the test with the 'dead-weight' testing frame. All tests were performed at 950˚C.

Once ruptured, macroscopic images of the fractured specimens were taken. The discs were then mounted on a stub and stage using a carbon sticker and imaged using a scanning electron microscope (SEM), both from a macro and microstructural point of view. Fracture surfaces in particular were imaged at high magnifications in order to help gauge an understanding of the failure modes involved.

3. Results & Discussion

As previously mentioned, parameter selection is a vital staple within ALM which consequently influences microstructure and the presence, frequency and type of material discontinuities present. Mechanical property assessment utilising SPC testing was used in order to determine whether low, medium or high energy densities are optimal for creep performance. Figure 8 indicates that medium energy density (90-DOE, etc.) offers optimal performance with time to rupture being 21.5 hours as displayed in Table 2. In addition to this, 90-DOE-1-1 (low) exhibits the highest displacement before rupture. This, alongside the highest minimum displacement rate achieved of all tests ($0.045 mm.hr^{-1}$) suggests that it behaves as the most ductile of the 3 samples. It is these mechanisms together with the minimal frequency of material abnormalities in 90-DOE-1-1 that has led to this variant's superior resistance to creep deformation.

The comparison of various types of abnormalities and their detriment to mechanical properties can also be observed in Figure 9**.** High energy samples containing various forms of microcracking such as solidification and ductility dip cracking (90-DOE-2-1) can be compared and contrasted with low energy samples containing frequent voidage and porosity (90-DOE-3-1). Such a comparison indicates the influence of energy density on mechanical performance. As can be seen in Table 1, low energy densities tend to have a far more detrimental effect on creep performance than high energy densities, 16.1 hours in comparison to 2.8 hours. The most plausible explanation for this would be the one previously alluded to in the Materials and Methodology section. 90-DOE-3-1, despite being located within the processing window, contains frequent porosity and voidage in comparison to its higher energy counterpart. This occurs as a result of the energy input per unit area not being sufficient enough to melt all the powder, leading to lack of powder consolidation. Subsequently, there is a deficit in performance as the presence of porosity and voidage act as both initiation sites and stress concentrations. On the other hand, 90-DOE-2-1 contains frequent microcracking which although do act as a detriment to mechanical properties as can be seen, is nowhere near as substantial. As previously mentioned, macro images were taken using an optical microscope, where Figures 10a, b and c showcase the increasing severity of cracking and rupture.

Table 1. Mechanical property data gathered from SPC testing for low, medium and high energy densities.

Sample ID	Load [N]	Temperature [°C]	Time to Rupture [hours]	Minimum displacement rate [$mm.hr^{-1}$]
90-DOE-1-1	150	950	21.5	0.045
90-DOE-2-1	150	950	16.1	0.041
90-DOE-3-1	150	950	2.8	0.147

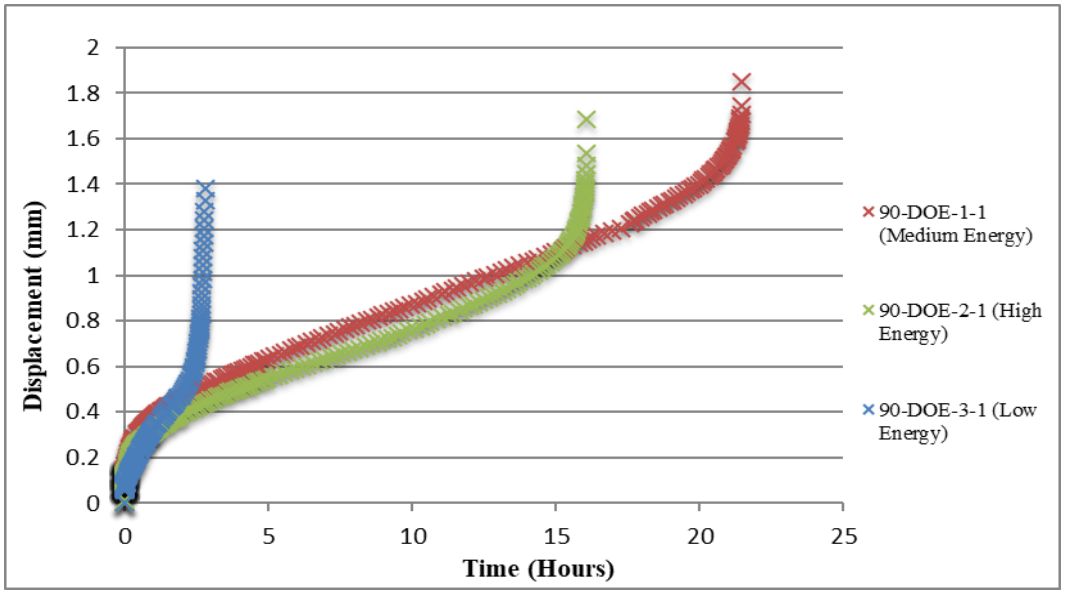

Figure 8. A direct contrast of parameter sets (low, medium and high energy densities) influence on creep performance.

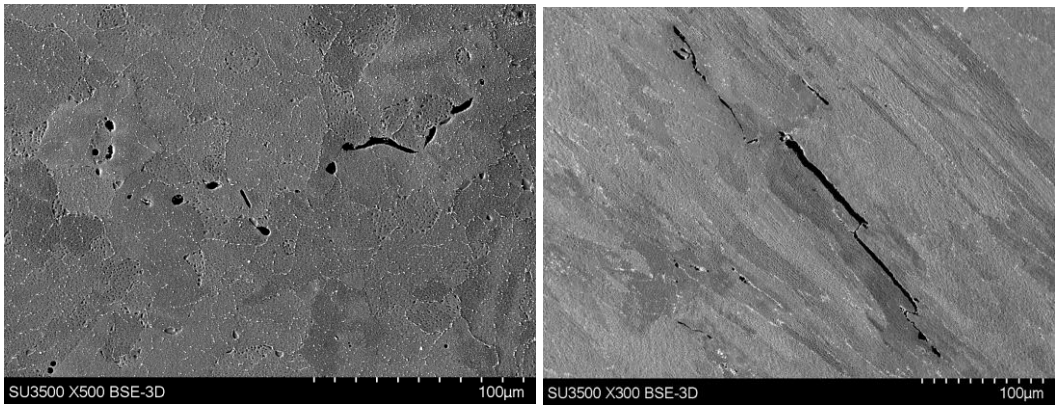

Figure 9. Back-scattered electron imaging of 90-DOE-3-1 (left) and 90-DOE-2-1 (right).

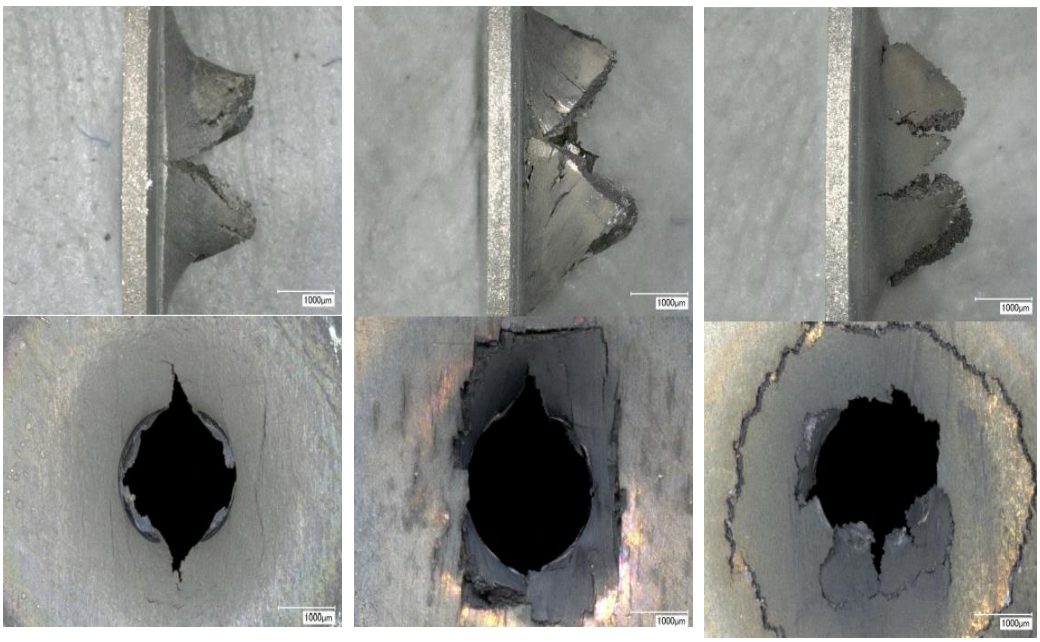

Figure 10. Optimal microscopy of samples **a)** 90-DOE-1-1, **b)** 90-DOE-2-1, **c)** 90-DOE-3-1.

In addition to parameter selection, Figure 11 emphasises and highlights the range of scatter that can be seen in separate builds, despite the same parameter set being used. Table 2 indicates that this scatter is as much as 3-fold, with the minimum time to rupture being 21.5 hours seen in 90-DOE-1-1 and the maximum being 59.2 hours for 90-DOE-1-3. Regardless of the same parameters and post manufacture processing utilised, the most plausible explanation for this would be down to the elastic heterogeneity of the microstructure. SPC testing utilises a small volume of material for its specimens, specifically 9.5mm diameter and 0.5mm thickness. As a result of this, the methodology is specifically sensitive in picking up these variations within localised regions of microstructure. Despite the similarity in columnar grain structures, Table 3 showcases the 90-DOE-1-1 sample picking up a higher volume of clustered fine columnar grains, giving rise to creep detrimental qualities giving the increased volume of grain boundaries. Conversely, 90-DOE-1-3s grains are indicated as being generally coarser. In addition to this, Figure 12 indicates that the 90-DOE-1-1's specimen has picked up a higher occurrence of porosity, in larger sizes, which in some cases are located at grain boundaries. This is in direct contrast to 90-DOE-1-3, where the lower volumes of smaller porosity are located within the grains. Given the small volume of material and heterogeneity of the sample, specimens may pick up differing volumes of extremely detrimental material defects that could act as stress raisers, inhibiting creep resistance and as a result leading to high scatter in data. Table 2 supports this proposed mechanism as being a major influencer in the particularly high minimum displacement rate seen in 90-DOE-1-1 suggesting that the porosity found has accelerated plastic deformation.

Table 2. Mechanical property data gathered from SPCT for varying build numbers at 90˚, parameter set 1.

Sample ID	Load [N]	Temperature [°C]	Time to Rupture [hours]	Minimum Displacement Rate [mm.hr-1]
90-DOE-**1-1**	150	950	21.5	0.045
90-DOE-**1-2**	150	950	30.5	0.027
90-DOE-**1-3**	150	950	59.2	0.019
90-DOE-**1-4**	150	950	39.7	0.026
90-DOE-**1-5**	150	950	46.0	0.020
90-DOE-**1-6**	150	950	42.8	0.024

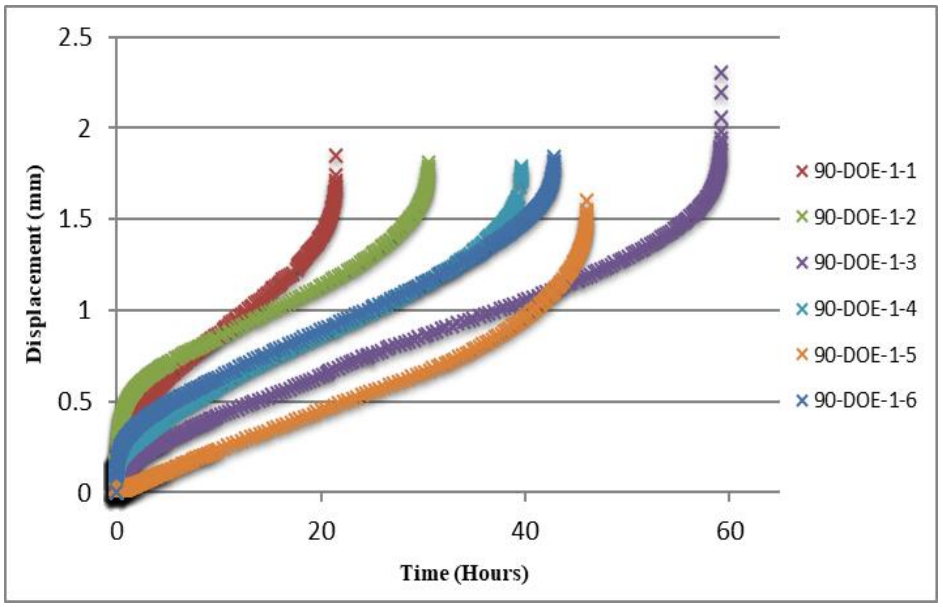

Figure 11. A comparison of the effect of build number on creep life for a 90º build parameter set 1.

Table 3: Grain size measurements of 90-DOE-1-1 in comparison to 90-DOE-1-3.

Sample	Average Grain Length (μm)	Average Grain Width (μm)
90-DOE-1-1	208.81	24.90
90-DOE-1-3	294.47	30.19

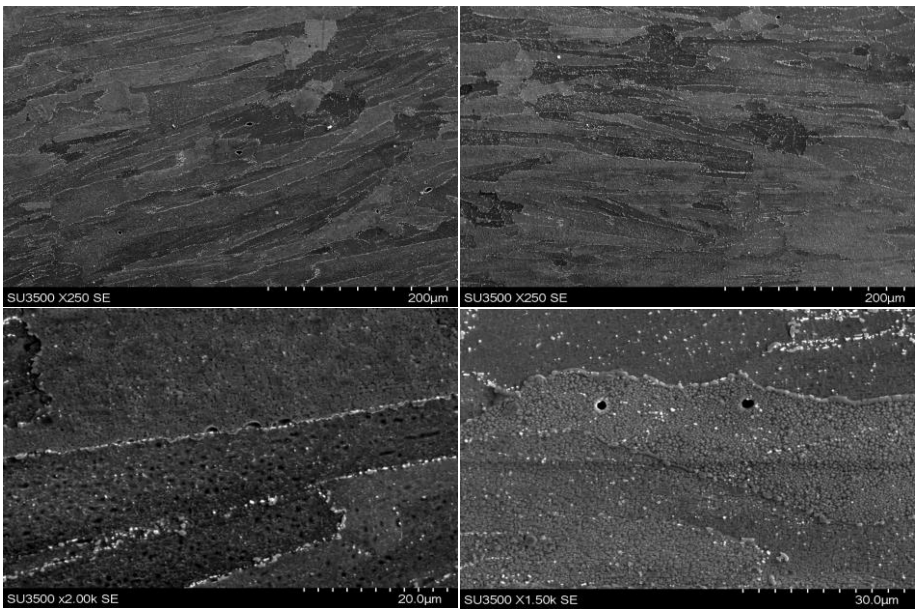

Figure 12. 90-DOE-1-1at low and high magnification (left), 90-DOE-1-3 at low and high magnification (right).

Moreover, post rupture fractography as shown in Figure 13 highlights the distinctly different fracture surfaces and as a result, the contrasting failure mechanisms. 90-DOE-1-1's fracture surface displays faceted features, suggesting that a brittle transgranular failure has taken place. This further supports its relatively high minimum displacement rate as brittle failures are known to be more instantaneous and as a result catastrophic.

90-DOE-1-3s failure could not be distinguished as to whether it was intergranular or transgranular as a result of oxycarbide formation along the fracture surface. Given the improved lifetime of 90-DOE-1-3, it is hypothesised that these oxycarbides can further aid grain boundary pinning, further aiding an enhancement in creep life and as a result explaining both the slow onset of minimum displacement rate and high final displacement value before rupture.

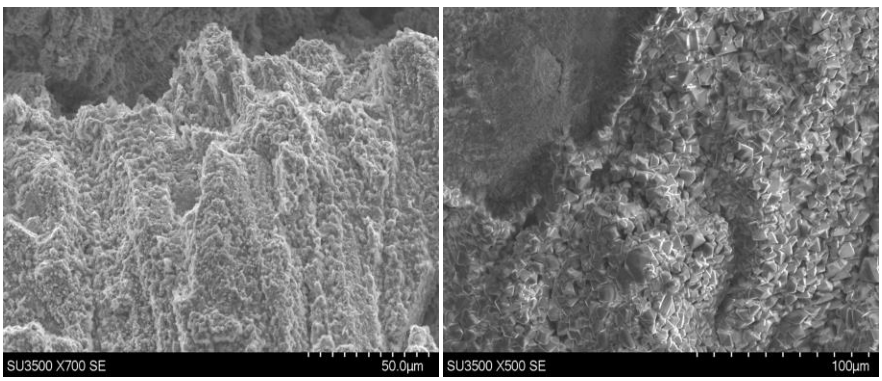

Figure 13. 90-DOE-1-1s brittle faceted fracture surface (left), 90-DOE-1-3s ductile dimpled fracture surface (right).

In addition to parameter sets and build variations, build orientation is shown to have a major influence in the mechanical performance of these samples, where Figure 14 highlights a major drop in time to rupture between 30° and 90° builds, irrespective to build number variation. Table 4 highlights this remarkable drop of 18.2 hours in lifetime between 90-DOE-1-1 & 30-DOE-1-1, alongside a staggering 56.2 hour drop between 90-DOE-1-3 and 30-DOE-1-3. This can be explained from a microstructural perspective, where under stress and specifically creep

deformation, cavities form at boundaries. Within the 30° builds, the microstructure is equiaxed in relation to the transverse direction as seen in Figure 15 and subsequently grain boundaries are typically located parallel to the stress orientation induced during SPC testing. As a result of this, these boundaries are subject to more load given both the higher volume of grain boundaries and the fact that grain boundary sliding is encouraged. Therefore, cavitations are set to coalesce quicker, resulting in lower rupture times and higher minimum displacement rates as shown. Given the higher minimum displacement rate, it would be expected that the 30° build displays a severely faceted fracture surface which can be validated in Figure 16.

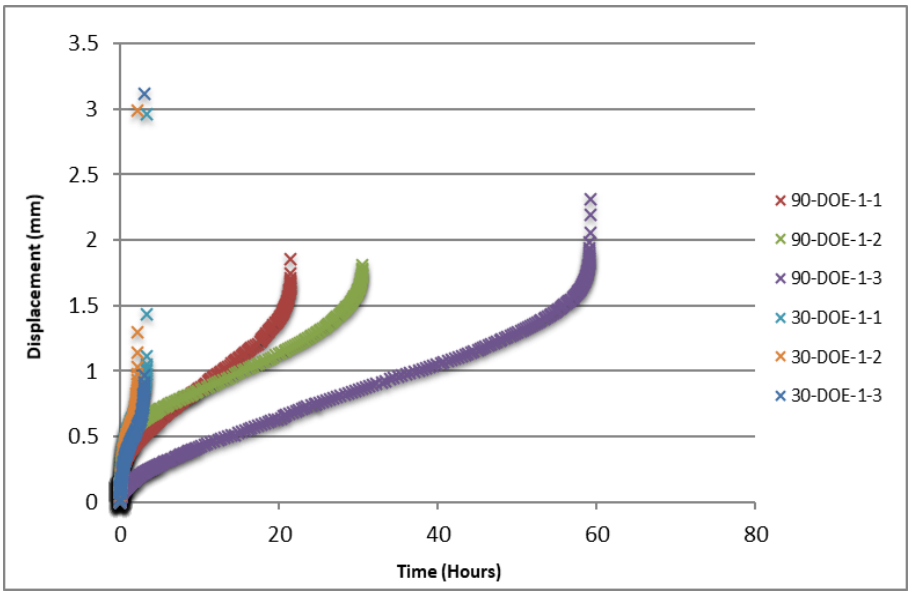

Figure 14. Effect of build orientation on creep properties for parameter set 1, build numbers 1-3.

Table 4. Mechanical property data gathered from SPCT for 30 and 90° builds orientations.

Sample ID	Load [N]	Temperature [°C]	Time to Rupture [Hours]	Minimum displacement rate [mm.hr^{-1}]
90-DOE-1-1	150	950	21.5	0.045
90-DOE-1-2	150	950	30.5	0.027
90-DOE-1-3	150	950	59.2	0.019
30-DOE-1-1	150	950	3.3	0.135
30-DOE-1-2	150	950	2.2	0.169
30-DOE-1-3	150	950	3.0	0.128

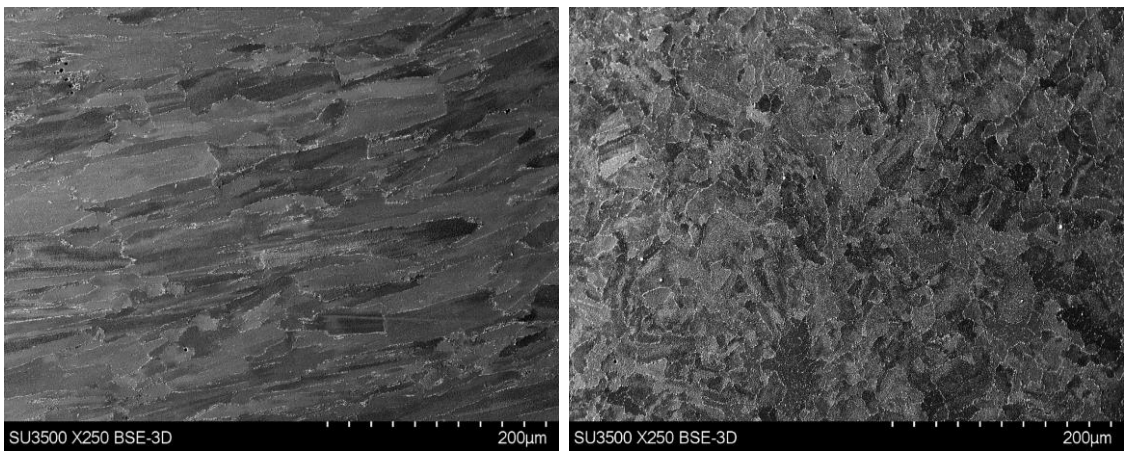

Figure 15. 90-DOE-1-1s columnar grain structure (left) and 30-DOE-1-1s equiaxed grain structure. (right).

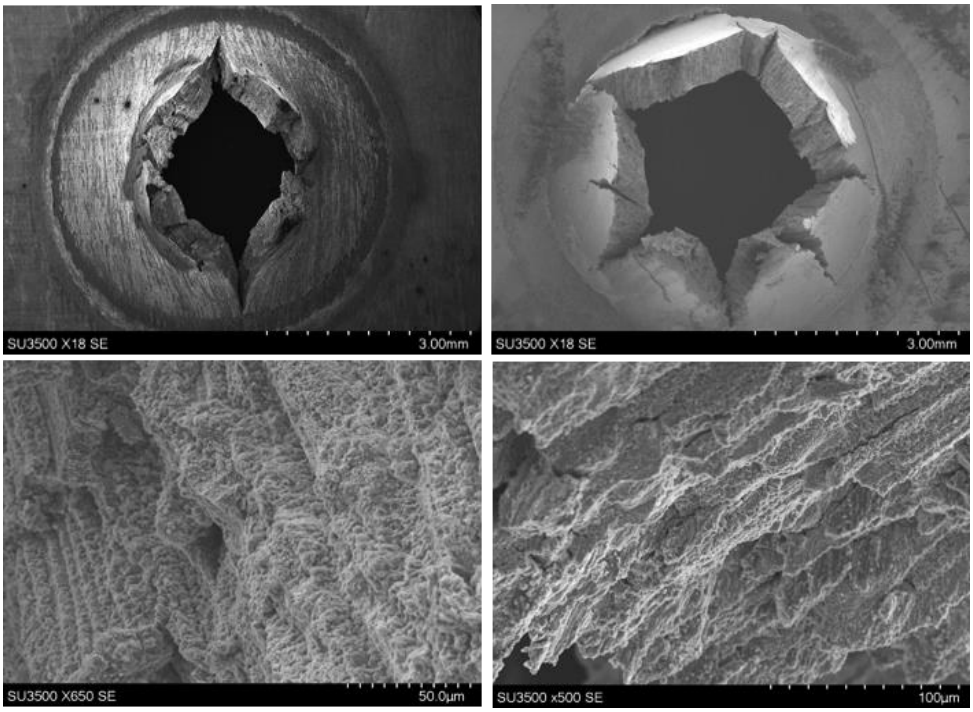

Figure 16. Fracture surface images of 90-DOE-1-1 at low and high magnifications (left side). Fracture surface images of 30-DOE-1-1 at low and high magnifications (right side).

4. Conclusions

The investigation of additively manufactured high gamma prime nickel superalloys with various process parameters and variables were investigated both microstructurally and mechanically utilising the small punch creep test. It has been shown that energy density has a considerable impact on both the type and size of microstructural discontinuities present through differing mechanisms. Porosity and voids attributed to low energy densities in particular have been shown to be severely more detrimental to mechanical properties than microcracking mechanisms accredited to high energy densities.

In addition to the differing parameter sets, the inconsistency of mechanical properties and microstructures between builds fabricated using the same processing variables has also been picked up utilising small punch creep testing. It is believed that this occurs due to the elastic heterogeneity of the samples microsctructure, where localised regions of differing microstructure have been picked up. In addition to this, given the small volume of material used in this methodology, results are subject to the sensitivity of material abnormalities such as porosity picked up within the specimens, giving rise to scatter. Fractography displayed contrasting failure modes between the best and worst performing build numbers, with 90-DOE-1-1 showcasing a brittle transgranular fracture and 90-DOE-1-3s failure displaying oxycarbides which indicated a grain boundary pinning/strengthening mechanism.

Finally, a comparison of samples fabricated at 30˚ and 90˚ build orientation was conducted. The creep resistance of 30˚ builds were significantly degraded as a result of their grain boundaries being oriented parallel to the loading axis induced during SPC testing. This gives rise to accelerated coalescence of cavitations and consequently faster creep deformation at an accelerated minimum displacement rate of $0.135 mm.hr^{-1}$ in comparison to $0.045 mm.hr^{-1}$. Fractography of these samples indicated that the 30˚ builds displayed more severe brittle transgranular fracture.

Acknowledgments: The current research was funded by EPSRC Rolls-Royce Strategic Partnership in Structural Metallic Systems for Gas Turbines (grants EP/H500383/1 and EP/H022309/1) alongside The Materials and Manufacturing Academy (M2A) supported through the European Social Fund. The provision of materials and supporting information from Rolls-Royce plc is gratefully acknowledged. Mechanical tests were performed at Swansea Materials Research and Testing Ltd. (SMaRT).

References

1. Pollock, T.R.; Tin, S. “Nickel based superalloys for advanced turbine engines: chemistry, microstructure and properties,” J. Propuls. power, vol. 22, no. 2, pp. 361–374, 2006.
2. Reed, R.C. The Superalloys, Fundamentals and Applications, vol. 53, no. 9. 2006.
3. Kozar, R.W.; Suzuki, A.; Milligan, W.W.; Schirra, J.J.; Savage, M.F. “Strengthening Mechanisms in Polycrystalline Multimodal Nickel-Base Superalloys,” 2009.
4. Donachie, M.; Donachie, S. Superalloys: A Technical Guide, 2nd Edition. ASM International, 2002.
5. Gokhare, V.G. “A review paper on 3D-Printing aspects and various processes used in the 3D-Printing,” vol. 6, no. 6, pp. 953–959, 2017.
6. Carter, L.N.; Martin, C.; Withers, P.J.; Attallah, M.M. “The influence of the laser scan strategy on grain structure and cracking behaviour in SLM powder-bed fabricated nickel superalloy,” J. Alloys Compd., vol. 615, pp. 338–347, 2014.
7. Jeffs, S.; Lancaster, R.; Davies, S. “Effect of Build Orientation and Post Processing of a Direct Laser Deposited Nickel Superalloy as Determined by the Small Punch Creep Test,” Key Eng. Mater., vol. 734, no. April, pp. 128–136, 2017.
8. Thomas, M.; Baxter, G.J.; Todd, I. “Normalised model-based processing diagrams for additive layer manufacture of engineering alloys,” Acta Mater., vol. 108, pp. 26–35, 2016.
9. Carter, L.N.; Essa, K.; Attallah, M.M. “Optimisation of Selective Laser Melting for a High Temperature Ni-Superalloy” Rapid Prototyping Journal 21, 1-8, 2015.
10. Manahan, M.P.; Argon, A.S.; Harling, O.K. “The development of a miniaturizsed disk bend test for determination of post irradiation mechanical properties,” J. Nucl. Mater., vol. 104, pp. 1545–1550, 1981.
11. Parker, J.D.; James, J.D. “Disc-bend creep deformation behaviour of 1/2Cr1/2Mo1/4V low alloy steel,” in creep and fracture of engineering materials and structures, 1993, pp. 651–660.
12. Harris, K.; Erickson, G.L.; Schwer, R.E. “MAR M 247 Derivations - CM247LC Directionally Solidified Alloy - Properties and Performance,” pp. 221–230.
13. Thomas, M.; Baxter, G.J.; Todd, I. “Normalised model-based processing diagrams for additive layer manufacture of engineering alloys,” Acta Mater., vol. 108, pp. 26–35, 2016.
14. Carter, L.N.; Attallah, M.M., Reed, R. C. “Laser Powder Bed Fabrication of Nickel-Base Superalloys: Influence of Parameters; Characterisation, Quantification and Mitigation of Cracking,” in 12th International Symposium on Superalloys, 2012, pp. 577–586.
15. Hurst, R.C.; Lancaster; R.J.; Jeffs, S.; Bache, M.R. “The contribution of small punch testing towards the development of materials for aero-engine applications,” Theor. Appl. Fract. Mech., vol. 86, pp. 69–77, 2016.
16. Lancaster, R.J.; Davies, G.; Illsley, H.; Jeffs, S.; Baxter, G. Structural Integrity of an Electron Beam Melted Titanium Alloy, Article Materials 2016, 9(6), 470.
17. CEN Workshop Agreement CWA 15267, “European Code of Practise: Small Punch Test Method for Metallic Materials.” 2007.